Synthesis and Caracterization of Calcite/A-Quartz Nanoparticuls Thin Film Based on Ouargla Region Rocks

N. Mebrouki[a], L. Zenkhri[*,B], S. Tlili[c], S. Boudjemaa[d], H. Belkhalfa[e], L. Benmabrouk[a], M. Zaoui[b], M. L. Belfar[b].

[a]Univ Ouargla, Fac. Mathematics and Material Sciences, Lab. Radiation and Plasmas and Surface Physics Laboratory (LRPPS), Ouargla, Algeria.

[b]Univ Ouargla, Fac. Mathematics and Material Sciences, Lab. Valorisation and Promotion of Saharan Resources laboratory (VPRS), Ouargla, Algeria.

[c]Univ Ouargla, Fac.Mathematics and Material Sciences, Development of New and Renewable Energies in Arid and Saharan Zones, Ouargla, Algeria

[d]Univ Tlemcen, Fac. Sciences, Lab.Catalysis and Synthesis in Organic Chemistry, Tlemcen, Algeria.

[e]Univ Ouargla, Scientific and Technical Research Center in Physico-Chemical Analysis (CRAPC), Ouargla, Algeria.

Received: 01/2023 **Published: 02/2023**

Abstract

This study reports the chemical composition of seven sandstones (OH1-OH7), then their use as precursor for the hydrothermal synthetesis of mater in thin films form. Structure identification of the seven samples and thin films produced was conducted by means of the Infra-Red spectroscopy and X-ray diffraction to documenting a composition of sandstones avrage major of 86.86 % α-quartz and minor of 13.14 % calcite. Moreover SEM analysis revealed the presence of solid solution in the crystal lattice of six sandstones samples with trace amounts of Fe, Al, Ag, Na, K.. The syntherised thin films at different temperture are composed mainly of [90.66 % calcite 9.33 % α-quartz and 69 % α-quartz /31% Sodium Chloride]. The crystallite sizes of the sandstones were calculated and estimated to be nanometric.

Keywords : Sand stone, Thin film, glass substrat, hydrothermal synthesis, X-rays diffraction.

Tob Regul Sci. ™ 2023;9(1): 480-494
DOI: doi.org/10.18001/TRS.9.1.36

1. Introduction

Rocks are natural resources found all over the world, including deserts, mountains, and beaches. They have received some geomorphological studies that have focused on the shapes and types of rocks [1]. The rocks that make up the earth's crust are thought to be the source of minerals, as they are essentially an assemblage of various minerals. They can be broadly classified into three major divisions based on their mode of origin: The rocks are classified as sedimentary, metamorphic, or igneous [2-3]. Sedimentary rocks, like igneous rocks, are composed of a limited

number of minerals, namely quartz, carbonates, clay, and feldspar. Minerals are the building blocks of industries ranging from construction to manufacturing, agricultural technology, and cosmetics [4].

The rocks are studied to determine the formation of specific regions or to determine the stability of a specific region, such as whether it is affected by environmental problems such as radiation [5]. Several studies in various countries have been conducted to determine the concentration of natural radionuclides in rock samples [6]. The characteristics of rocks have been investigated in materials science using various methods [7-9] in micro structure as well as macro structure, which can describe the physical properties of rocks [10-11], and structural properties [5] [12-14]. Furthermore, information about rock minerals will provide rock properties [15].

Calcium carbonate ($CaCO_3$) is one of the most abundant materials on the planet, with several crystalline forms including calcite, aragonite, and vaterite [16]. after its first structure determination by W. L. Bragg in1924 [17]. This is due to the widespread abundance of aragonite and its important role in geochemistry and especially in biomineralization [18]. The calcite structure has the space group R3c [19], and its thin film has been fabricated by The orthorhombic polymorph of $CaCO_3$, which has captivated the attention of researchers for the past 95 years using a variety of methods as reported in [20-22]. Calcite is important in sedimentary environments and can be found in metamorphic, igneous, hydrothermal, and secondary mineralization. Aragonite and calcite are interesting because they can be found in a variety of geological environments [23]. These calcite minerals are frequently used as model compounds for studying structural sources of optical anisotropy [19].

Oxygen and silicon Quartz's two constituents (SiO_2) are two of the most abundant elements in the Earth's crust. Quartz exists in two polymorphic phases: -quartz and -quartz [24]. Quartz is found in rocks, soils, and sands, and it forms from molten magma at ~800 °C and underground hydrothermal veins at temperatures ranging from 250 to 450 °C [25]. Several methods have been proposed in the literature for producing quartz thin films [26-28]. Quartz is nearly 100% SiO2 chemically, and only a few elements can be incorporated into its crystallattice [29-32]. Because quartz is so common in igneous, metamorphic, and sedimentary rocks, several attempts have been made to use trace elements for genetic interpretation [33-36]. The goal of this work is to exploit natural resources (rocks) to be used as precursors for the hydrothermal synthesis of material in thin film form, because it contains expensive chemical elements and is not harmful to health or the environment.

2. Experimental

2.1. Materials and methods

The study site is located in north-eastern Algeria (Fig. 1), delimited by the longitude 5° 20’ E and the latitude 31° 57’ N exactly in the geographical position (31.802505.5395) with an average height of 137 m [37].

Fig. 1. *Location of the study area*

This region is characterized by high temperatures. The rocks were sampled in 2019 that exist on the surface. They were of different size, color and irregular shape, approximately 3 to 5 cm in length Fig. 2.

Fig. 2. *The samples of studied rocks*

The seven sandstones (OH1- OH7) were used as the source of metallic cations. Analytical graded chemicals including SrCO3, HNO3 (65%) and HCl (37%) was obtained from BIOCHEM. The substrates used to support the formed thin film were (0382-0004) Cito glass slides with a size of (75 × 25 × 1.1 $mm^{3)}$.

The collected rocks were washed, pollished by using Mecapol P 255 U device and thoroughly dried at room temperature, then crushed using Retsch device for few minutes (V= 950 rpm) to obtain a fine powder. Finaly the powder kept in a plastic box forafter use. Infrared spectroscopy (FTIR) is a simple method which can be used to identify the chemical bands from the organic, inorganic, crystalline or amorphous compound [38]. The FTIR measurements were carried out using an Agilente cary 660 FTIR spectrometer. The samples were scanned in a spectral range from 4000 to 400 cm^{-1}. Sample of the natural sandstones powder and the morphology of the $CaCO_3/SiO_2$ thin films were subjected to SEM-EDS analysis using TESCAN VEGA3 electron microscope. X-rays cristallgraphic data were collected on powdered samples at room temperature using a powder diffractometer BTX-716 and BRUKER-binary V3 with Cu Kα radiation at the wavelenght (λ = 1,5406 Å) radiation at room temperature. All samples were analysed from 5° to 55°- or 90° by a step of 0.0500 °/s, 0.019 °/s respectivelly,. The phasis structures were identified using the expert High Score Plus softward [38] configured with ASTM file.

2.2. Synthesis of ($CaCO_3$-SiO_2) thin films

The powdered rock samples with a mass of about 3 mg was soaked for 48 hours in mixture of 3 ml HNO_3 and 9 ml of HCl (aqua regia) at room temperature After two days we

extracted it. Then we took only 3 ml of it and extension by 15 ml of distilled water with 3 mg Serium carbonate ($SrCO_3$). The resulting mixture was put inside astainless-steel hydrothermal reactor which is containe a glass substrat at 150 °C, 200 °C, 250 °C and 300 °C respectively. After 2 hours the reactions mixture were cooled down at room temperature and the products were filtered off and washed with distilled water and aciton several times.

3. Results and Discussions

3.1. Characterisation of rocks

3.1.1. IR-spectroscopy of (OH1-OH7) samples

Figure 3 shows the spectra of the analyzed (OH1-OH7) samples respectively. The detail on the vibration bands assignments is summarized in table 1. The sharp absorption band between 1081.85-1096.83cm^{-1} has been observed and seems to fit with symmetrical stretching of Si–O–Si bond [40-45]. CHENGLI YAO (2013) *and* Flemming A. Andersen (1991) have *reported the* characteristic peaks at 1088 and 1090 cm^{-1}, indicating the emergence of calcite [43], and the vibrations of the carbonate ions [44], respectively. Whereas the absorption bands between 777.17-798.38 cm^{-1} have been observed and correspond to Si-O symmetrical bending vibration, which confirm the presence of α-quartz [40-41]. Other bands between 693.91-694.004 cm^{-1} coincide with Si–O–Si symmetrical bending. The 694.004 cm^{-1} band indicates that the quartz in the samples is crystalline [45]. The absorption peaks between 500-530 cm^{-1}, 467.13-483.19 cm^{-1}, 440.49-449.81cm^{-1} and 425.14-429.47 cm^{-1} due to the asymmetrical vibrations of Si-O-Al, symmetrical streching of the Si-O, asymmetrical bending of the Si-O-Si band and bending vibrations of Si-O-Fe, respectively [47-49]. Finaly, the peaks between 425.14-429.47 cm^{-1}, 440.49-449.81 cm^{-1}, 467.13-483.19 cm^{-1}, 693.91-694.004 cm^{-1} and 777.17-798.38 cm^{-1} indicate the presence of quartz in all rock samples. The characteristic peaks between 1081.85-1096.83 cm^{-1} and 2357.08-2361.79 cm^{-1} indicating the emergence of calcite in the whole samples except OH7 [40-41]. Form FTIR qualitative analysis, and by comparing our results with other studies, the obtained vibration bonds values are in good agreement with results carried out in the literature [40-43] which indicates that the most bands are attributed to quartz and calcite.

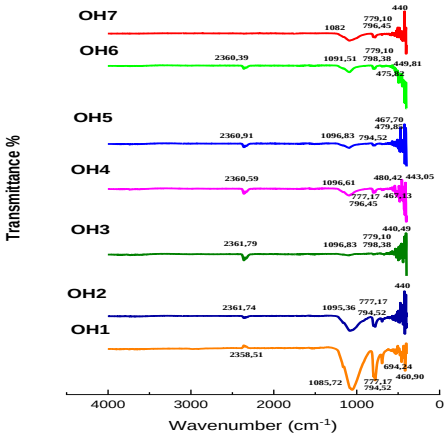

Fig. 3. FTIR absorption spectrum of OH sandstones.

Table 1*.The main bands of IR absorption and associated bond vibration of our samples.*

Band(cm^{-1})	Bond (vibration mode)	Compound
2357.08-2361.79	Indicating the emergence of	Calcite
1081.85-1096.83	calcite	Quartz
1088	Si–O–Si (symmetrical	Calcite
1090	stretching)	Calcite
777.17-798.38	Indicating the emergence of	Quartz
693.91-694.004	calcite	Quartz
694.004	vibrations of the carbonate ions	Quartz
467.13-483.19	Si-O (symmetrical bending	Quartz
440.49-449.81	vibration)	Quartz
425.14-429.47	Si–O–Si (symmetrical bending)	Quartz
	Quartz	
	Si-O (symmetrical streching)	
	Si-O-Si (asymmetrical bending)	
	Si-O-Fe (bending vibrations)	

3.1.2. Elemental analysis of (OH1-OH7) samples

The element concentrations obtained for the seven sandstones (OH1-OH7) are presented in the Table 2. The presence of the identical substantial elements (O, Si, C, Ca) in all the samples is a clear indication of the natural quartz/calcite structure of the rocks. While the specific trace metal (Fe, Al, Ag, Na, K) for each sample, with significant differences observed in their presence and concentrations shows that the quartz/calcite structure might be modifie. As reported by Shanling, Qing and Jun in data study of trace element distribution in hydrothermal quartz from southern China reveal that Al, Li, Na, and K are the most important elements in quartz [40], while Fe also can be embedded in the crystal lattice of calcite [51]. The variety of chemical composition for the seven rocks can explain the differences of their colors.

***Table 2** . Elemental analysis of OH sandstones.*

Samples	O (%)	Si (%)	C (%)	Fe (%)	Al (%)	Ag (%)	Na (%)	K (%)	Ca (%)
OH1	66.58	21.65	9.97	0.85	0.55	0.41			
OH 2	67.69	31.28		0.36	0.67				
OH 3	61.83	25.39	9.48	1.70	1.13		0.47		
OH 4	61.88	22.86	11.94	1.75	0.89				0.68
OH 5	68.66	24.51		0.74	2.98		1.77	0.90	0.44
OH 6	61.32	36.69		1.20	0.35				0.44
OH 7	61.87	1.46	19.54						17.14

3.1.3. X-ray diffraction analysis of (OH1-OH7) samples

The diffractometer measured in figure 4 exibite a strong diffraction peaks could be seen, indicating that OH sandstones have high crystalline nature, which agrees with the results of Meftah and Mahboub 2020 [52]. The results of the Xpert HighScore software matching (Table 3) revealed the presence of quartz in the majority and calcite in the rock samples.

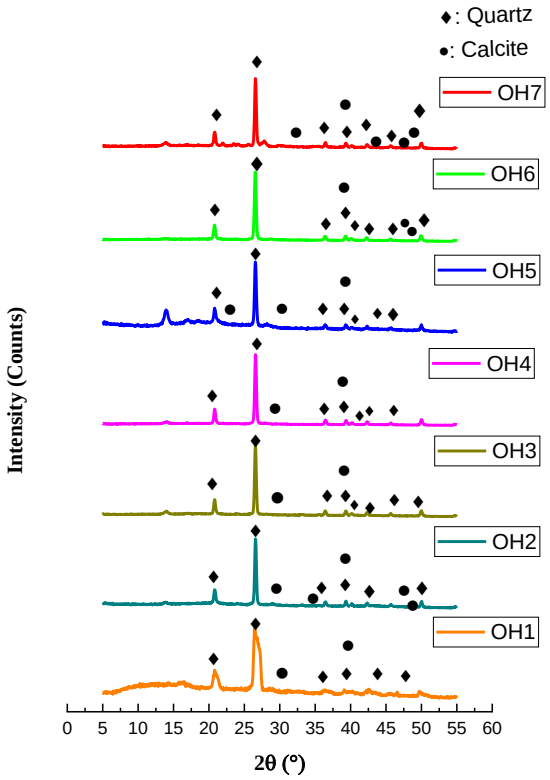

Fig. 4. The XRD pattern of OH2 sandstones.

Table 3. Indexed Powder XRD Pattern for OH2 sandstones.

2θ (°)	Intensity (a.u)	Mineral	(dhkl) cal (Å)	Hkl
20.7709	1556.38	Quartz	4.27305	100
26.5832	5789.14	Quartz	3.35048	101
29.2773	443.325	Calcite	3.04801	104
31.5967	324.419	Calcite	2.82935	006
35.8935	279.252	Calcite	2.49989	110
36.4035	635.429	Quartz	2.46603	110
39.3111	682.268	Quartz, Calcite	2.29007	102/113
40.2535	385.766	Quartz	2.23860	111
42.3029	555.187	Quartz	2.13477	200
47.1143	244.788	Calcite	1.92737	024
48.6941	221.515	Calcite	1.86847	116
49.9412	613.894	Quartz	1.82469	112

The d_{hkl} inter-planar spacing has been calculated from the X-ray diffraction profile using the Bragg law:

$$2d_{hkl}sin\theta = n\lambda \quad (1)$$

Where θ is the diffraction angle, λ is the used wavelength of X-rays and n is the order of

diffraction.
We note that the calculated value of d_{hkl}-spacing (Table 3) matched very well with those of the standard JCPDS data. The lattice constants a, b and c, for the hexagonal and rhombohedral phase structure was determined from XRD results using the following equation [59]:

$$\frac{1}{d_{hkl}^{\ 2}} = \frac{3}{4}\left(\frac{h^2 + hk + k^2}{a^2}\right) + \frac{1}{c^2}^{\ 2} \quad (2)$$

Where (h k l) are the Miller indexes and 'a', 'c'are the lattice constants.
The calculated and standard JCPDS lattice constants for quartz and calcite are indicated in Table 4. The calculated lattice parameters for the quartz (a = b = 4.93206 Å and c = 5.4741 Å) and calcite (a = b = 4.99978 Å and c = 16.9761 Å) agree well with the standard values (a_0 and c_0). The samples crystallite sizes were calculate from the strongest peaks by using Scherrer's formula [60]:

$$D = \frac{0.96\lambda}{\beta \cos\theta} \quad (3)$$

Where D is the crystallite size, λ (=1.5406 Å) is the wavelength of X-rays, β is the width full at half maximum (FWHM) of the most intense diffraction peak, usually measured in radian and θ is the Bragg angle.

Table 4. *Lattice parameters a, c and crystalline size D of quartz and calcite of OH sandstones.*

Mineral	Standard lattice parameters (Å)	Calculated lattice parameters (Å)				FWHM (°)	Crystalline sizes (nm) (D)
		a	Δa = a_0-a	c	Δc = c_0-c		
Quartz (SiO2)	a_0 = 4.9134[a] c_0 = 5.4052[a]	4.93206	-0.0187	5.4741	–0.0689	0.18	35.44
Calcite (CaCO3)	a_0 = 4.9890[b] c_0 = 17.0620[b]	4.99978	-0.01078	16.9761	0.0859	0.36	43.4

[a]data from JCPDS (N° 46–1045)
[b]data from JCPDS (N° 05–0586)

By matching the observed XRD peaks (Fig. 4) with ASTM cards, some notes can be recorded:

The peaks positioned at 2θ =20.7709°, 26.5832°, 36.4035°, 39.3111°, 40.2535°, 42.3029° and 49.9412° corresponding, respectively, to the planes (100), (101), (110), (102), (111), (200) and (112) are due to the hexagonal crystal structure of SiO_2 (α-quartz), under the space group P3221 (154) which is consistent with JCPDS file (N° 00-046–1045) [52] with a lattice parameters of a = b = 4.9134 Å and c = 5.4052 Å. Whereas diffractionsat 2θ= 29.2773°, 31.5967°, 35.8935°, 39.3111°, 47.1143° and 48.6941°, for the crystalline planes (104), (006), (110), (113), (024) and (116), respectively. These planes fit calcite ($CaCO_3$) compound as reported by JCPDS (N°

00-005-0586) with a rhombohedral crystal system belonging to R3c (167) space group [52-54] with a = b = 4.99978 Å and c = 16.9761 Å.

Quartz is characterized by its strongest, highest intensity and prominent diffraction at 2θ = 26.5832° diffractionsand the highest intensity and prominent of calcite is at 2θ =29.2773. In addition, the right or left shifts observed at the 2θ positions of the peaks (26.5832°, 26.5548°, 26.5773°, 26.5544°, 26.5409°, 26.5598°) in whole samples can be attributed to the presence different percentages of metal traces in the crystal lattice of the rocks, called defects, which affect the crystal size and hence the d-spacing between lattice planes. The metal traces can occupy the sites of substitution atoms or can be interstitial if they are small [56-57]. It is confirmed by both EDS and FT-IR analysis results for Si-O-Al at 500-530 cm^{-1} and Si-O-Fe at 425.14-429.47 cm^{-1} as shown above.

From Table 3 the spacing distances d_{hkl} of 4.27305, 3.35048 and 2.46603 (Å) / 3.04801, 2.82935 and 2.49989 (Å) affirm the presence of the α-quartz phase in our rock[40][58] and calcite, respectively. By the same way, the same calculations were made for all the rocks to obtain information that proves the same results. The α-quartz is the most stable phase of quartz at room temperature.

The crystallite size of quartz D = 19.94 (OH1), 35.44 (OH2), 24.66 (OH3), 24.79 (OH4), 33.80 (OH5), 25.24 (OH6), 26.33 (OH7) nm whereas the crystallite size of calcite D = 13.85 (OH1), 43.40 (OH2), 22.88 (OH3), 30.75 (OH4), 38.18 (OH5), 41.48 (OH6), 27.65(OH7) nm, both of them remain less than 100 nm which makes it of great interest to the nanometric industries and nanotechnologies.

3.2. Caracterization of calcite/α-quartz thin films

3.2.1. IR-spectroscopy of calcite/α-quartz thin films

Fig. 5 show FTIR spectra of the thin films synthesised at 150°C, 200°C, 250°C and 300°C and the vibration bands assignments detail are summarized in table 5. The absorption bands observed at 428.11, 524.54 and 983.73 cm^{-1} are indicating the presence of quartz in all thin films [46-47]. The characteristic peaks at 711.60, 875.52, 1430.92 and 2354.66 cm^{-1} attributed to the CO_3^{-2} ion, indicating the presence of calcite in the whole thin films [43][45][61].

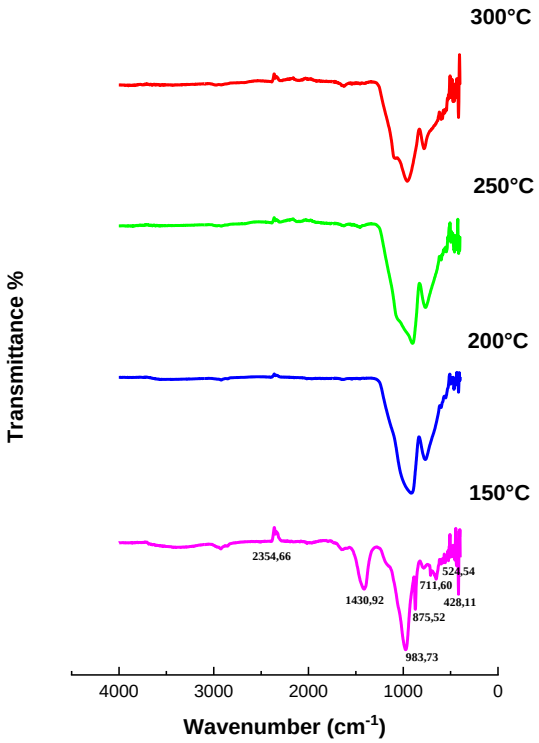

Fig. 5. *FTIR absorption spectrum of our thin films.*

Table 5. *The main bands of IR absorption and associated bond vibration of our thin films.*

Wavenumber (cm^{-1})		Assignement
Calcite	Quartz	
	428.11	Si-O-Fe bending vibrations
	524.54	Si-O-Al asymmetrical vibrations
711.60		CO_3^{-2} (in-plane bending)
875.52		CO_3^{-2}(out-of-plane bending)
983.73		The vibration of quartz
1430.92		CO_3^{-2} Asymmetrical stretching vibrations
2354.66		Calcite

The peaks at 428.11, 524.54 and 983.73 cm^{-1} are assigned, respectively, to Si-O-Fe, Si-O-Al lattice flexing vibrations [47] and bending vibrations [48-49] and the absorption band at 983.73 cm^{-1} attributable to the vibration of quartz [61]. The absorption band at 2354.66 $cm^{-1}$is specified at 150 °C, its mode of movoument vibrations of the band was not specified [42]. The absorption band at 1430.92 cm^{-1} refers to the asymmetrical stretching vibrationsof the carbonate ion CO_3^{-2}, while the 875.52 cm^{-1}band is assigned to the out-of-plane bending, whereas, the 711.60 cm^{-1} band is assigned to its in-plane bending [61].

3.2.2. Morphological analysis of calcite/α-quartz thin films

The surface morphology of calcite/α-quartz thin films synthesized on the glass substrate at different temperatures are shown in Figure 6 (a), (b), (c) and (d) respectively. At 150 °C, 250 °C and 300 °C, the surface morphologies of the $CaCO_3$ thin films are thin, wool-like bristles, circular disk-shaped and of unspecified thickness and scattered pieces with irregular structure, respectively. While the SiO_2 thin films at 150 °C, 200 °C and 300 °C are a substance in the form of grains and have approximately the same size of particles that reflect light, while SiO_2 at 250 °C has a mass of particles with approximately different size. At 200 °C, the NaCl thin films are a regular particle with a smooth surface. We conclude that the optimal temperature to obtain a thin calcite films is 250°C and the morphology of our films prepared by hydrothermal synthesis is temperature dependent.

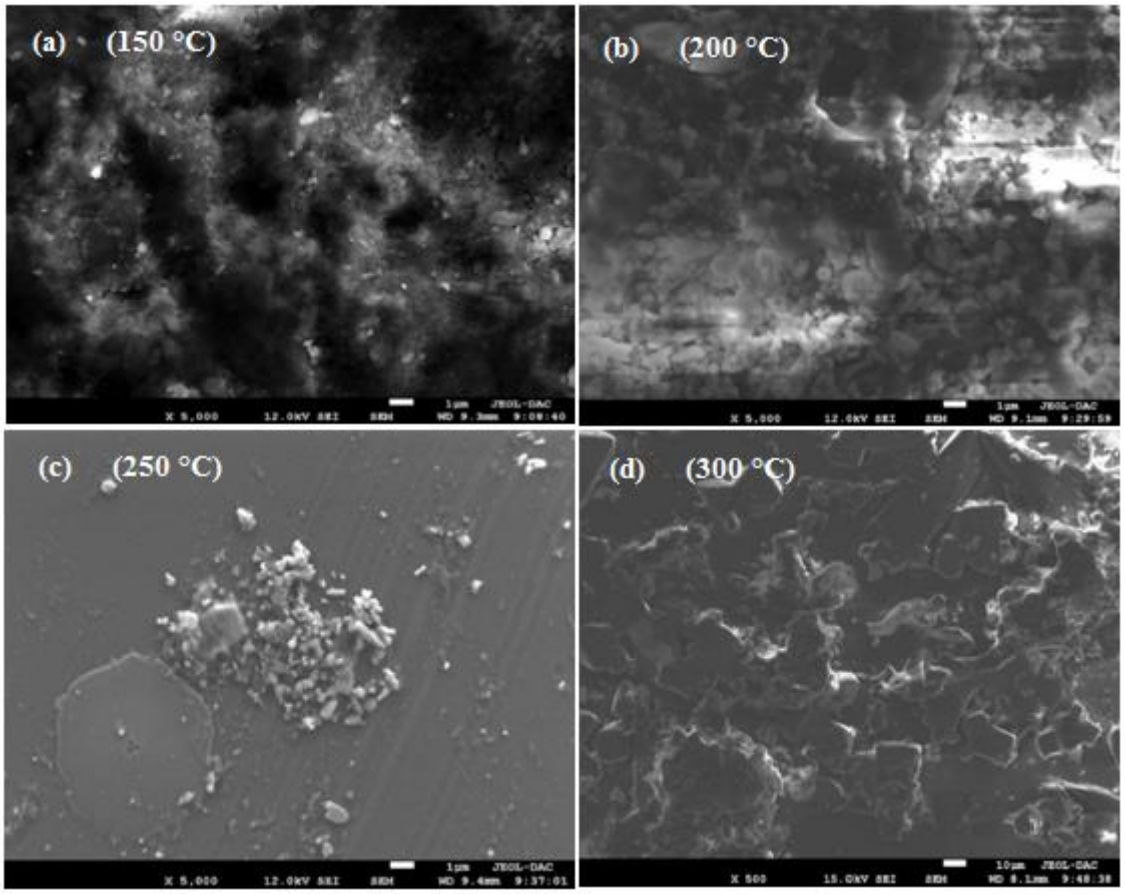

Fig. 6. *SEM images of thin films at 150°C (a), 200°C (b), 250°C (c) and 300°C (d).*

3.2.3. Elemental analysis of calcite/α-quartz thin films

Table 6. gathers EDS results representative peaks for O, Si, and Ca for all the samples at 150 °C, 200 °C and 300 °C. The $CaCO_3/SiO_2$ thin films show similar peaks corresponding to the spectra of $SiO_2/CaCO_3$, which indicate a successful formation of $CaCO_3/SiO_2$ thin films.

Table 6. *Elemental analysis of synthesis thin films at different temperatures.*

Thin films	O %	Si %	Ca %	Na %	Al %	Ag %	Mg %	P %
150°C	69.267	14.521	4.476	5.503	0.963	0.205	5.065	
200°C	30.278	15.796	8.466	22.156	2.392	5.186	2.376	13.351
300°C	69.594	10.161	2.601	8.418	0.484	0.581	6.649	1.512

3.2.4. X-ray diffraction of calcite/α-quartz thin films

XRD patterns of the thin films formed at different temperatures are presented in Fig. 7. The observed peaks at 150 °C, 250 °C and 300 °C are matched with ASTM file (N° 00-005-0586) and (N° 00-046-1045) forms the ($CaCO_3/SiO_2$) with ratio (98/2), (89/11) and (85/15) respectively. Furthermore, at 200 °C forms the (SiO_2/NaCl) ASTM file(N° 00-005-0628)with (69/31) ratio.

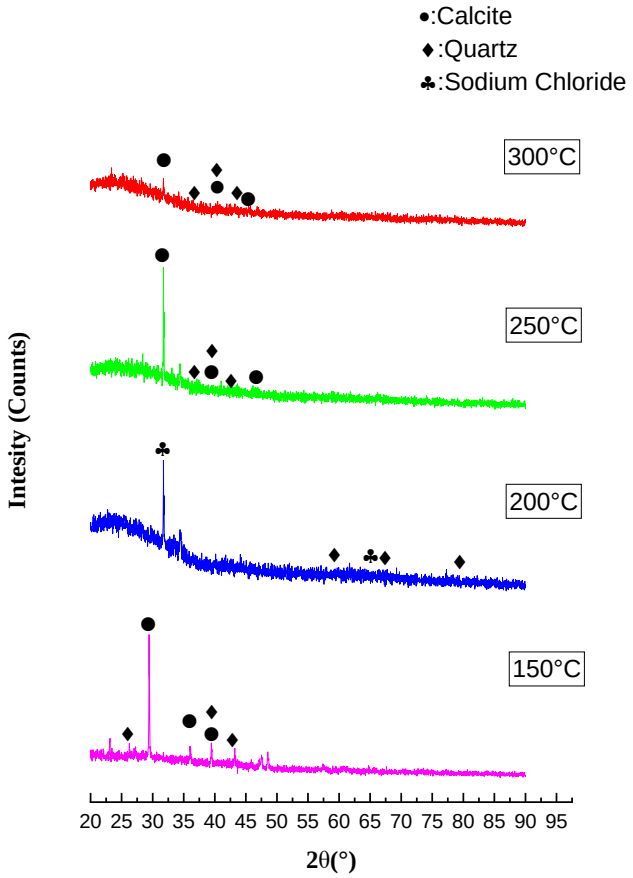

Fig. 7. *The XRD pattern of our thin films.*

Whereas, the reaction temperature increased to 250 °C then to 300 °C, the intense peaks at 2θ = 29.4104° (150 °C) of the calcite phase [56] has shifted to 31.67. This is an expected shift given the traces elements anchored to the crystal lattice previously reported by SEM-EDS analysis as different types and values, and this may be the slight too to the deformation of the crystal lattice due to temperature. By the same, at 150 °C the pattern exhibited the peak

diffraction (2θ) near 36.0435 of the calcite cristallization, while at 250 °C (36.4899) and 300 °C (36.4412) reflect to quartz. The peak at 2θ =39.0435° (150 °C), 39.4120° (250 °C) and 39.6531° (300 °C), respectively, reflect the existence of calcite as reports in [55,57] and the existence of quartz phases at the same time as reports in. [62,63].

There are also another peaks for quartz / calcite 42.3904° (150 °C) 42.1719°/47.1827° (250 °C), 42.4828°/43.2101° (300°C), 59.9443°, 67.7348° and 80.6060° (200°C). At 200°C the thin films also contains NaCl which exhibits two intense peaks at 2θ = (31.7266° and 66.1949°). These two peaks correspond respectively to the (200) plane and its harmonic (400) are due to the cubic system with the Fm3m symmetry space group as reported in the JCPDS (N° 00-005-0628 card) [64] with a = b = c = 5.636176 Å. While the decrease in the intensity of the peaks when the heat of reaction increases indicates that the good crystallization takes place at 150 °C.

The results show the synthesis of the thin films of calcite and quartz at reaction's different temperature, except that at 200°C there is no calcite present. The presence of specific trace metals for each sample, with significant differences observed in their presence and concentrations, indicates that the quartz/calcite structure may be modified as reported in the previous analysis (EDS) and this may be the slight Shift in explained position of the spectra due to different radii from mineral bead to mineral bead.

The crystallite size of quartz D = 113.63 (150 °C), 116.05 (200 °C), 101.27 (250 °C), 109.07 (300 °C) nm

whereas the crystallite size of calcite D = 65.68 (150 °C), 101.98 (250 °C), 121.77 (300 °C) nm and the crystallite size of Sodium Chloride D = 97.08 (200 °C) nm, Therefore, the quartz and calcite thin films are not nanometric at all reaction temperatures, except that at 150 °C the calcite thin films and at 200 °C the Sodium Chloride thin films are less than 100 nm, making them of great interest to the nanometric industries and nanotechnologies.

4. Conclusions

Calcite/α-quartz thin films were successfully prepared using hydrothermal method where the mean precursors were from natural source. Sandstones could be important sources of quartz and calcite which are primary materials for many industrial applications. IR, SEM-EDS and XRD show that OH sandstones mainly consists of about 86.86% quartz in α- phase, minor calcite mineral (about 13.14%) and some trace elements (Al, Fe, Na, Ag, K), this indicates a high purity of the quartz and calcite of these sandstonesand their thin films. the sandstones of Ouargla region are very rich in quartz with hexagonal crystal structure. In addition, the rock has some calcite with a rhombohedral crystal system.

The crystallite sizes of quartz and calcite are D = 27.17 and 31.17 nm, respectively, demonstrating the nanometric aspect of the Ouargla region sandstones, that can be used in nanometric industries and nanotechnologies.

After the success of converting the nanoscale raw material (SiO_2/$CaCO_3$) into a non-nanoscale thin film, as a future prospect, we will try to improve the particle size of the thin

films to successfully produce them from a natural material by changing the experimental conditions, to make quartz thin films on a nanoscale and with piezoelectric properties from natural precursor rocks known to possess these properties, which can not be used in the industrial and nanotechnology fields, and therefore transform them to thin films can be used. Since for calcite, 150°C or less is considered optimum to obtain nano-scale thin calcite thinfilms which were nanometer crystal grains. At 250 °C, calcite was a continuous thin film, cohesive and crystallized, but not on a nanoscale, the development of thin films.

Acknowledgments

The authors gratefully acknowledge the assistance of everyone in the completion of this work. Sincere thanks are extended to Pr. Gheriani Rachid and Pr. Hesseni Messoud. Thin film laboratory, Mohamed Khider University of Biskra, Algeria; Sahara geology laboratory (E1521600 Lab. DAC-HR University of Setif 1; Laboratory of Radiation and Plasmas and Surface Physics (LRPPS); and the Physics Department at the University of Ouargla, Algeria.

References

[1] P. S. Nayak , B. K. Singh , Bulletin Materials Science **30** (3), 235 (2007).
[2] V. Chander , D. Tewari , V. Negi , R. Singh , K. Upadhyaya , L. Aleya , Science of the Total Environment **748,** 141269 (2020).
[3] J. A. Aidekoya , International Journal of Physics Science 613, (1995).
[4] H. King, Geology community 2005 (2015).
[5] A. H. Al-Ghamdi , Journal of Radiation Research and Applied Sciences **12** (1), 87 (2019).
[6] F. B. Masok , P. L. Masiteng , R. D. Mavunda , P. P. Maleka , H. Winkler , Journal of Radiation Research and Applied Sciences **11**, 29 (2018).
[7] T. Rahman , L. Maxim , Z. Yihuai , B. Ahmed , I. Stefan , 13th International Conference on Greenhouse Gas Control Technologies **114**, 5023 (2017).
[8] Z. A. Ahmed , L. Maxim , J. V. Sarah , L. J. Michael , B. Ahmed , I. Stefan , Journal of Petroleum Science and Engineering **129**, 48 (2015).
[9] D. Zandomeneghi , M. Voltolini , L. Mancini , F. Brun , D. Dreossi , M. Polacci , Geosphere **6** (6), 793 (2010).
[10] M. Arif , B. Ahmed , L. Maxim , I. Stefan , Energy Procedia **114**, 4832 (2017).
[11] T. Rahman , L. Maxim , B. Ahmed , I. Stefan , Journal of Colloid and Interface **469**, 63 (2016).
[12] I. R. AL-Homadi , I. S. Al-Okli , The All-Earth Iraqi National Assembly, Al-Mujjad **18**(1), 149 (2018).
[13] T. A. M. Mohammed , International Journal of Basic and Applied Sciences IJBAS-IJENS **12**(06), 109 (2012).
[14] D. A. Mckeown , E. P. Jeffrey , American Mineralogist **86**, 701 (2001).
[15] M. R. Setiawan , M. Iqbal , R. N. Siregar , Journal of Science and Applicative Technology **206** (2018).
[16] J.H. Bang , Y.N. Jang , K.S. Song , C.W. Jeon , W. Kim , M.G. Lee , S.J. Park , Effects of sodium laurylsulfate on crystal structure of calcite formed from mixed solutions, Journal Colloid Interface Science **1**, 356 (2011).
[17] W. L. Bragg , F.R.S. Langworthy , Proc. R. Soc. A, **105**, 16 (1924).
[18] E. N. Caspi, B. Pokroy, P. L. Lee, J. P. Quintana , E. Zolotoyabko , ActaCrystallgraphica section

B **61**,129 (2005).
[19] E. N. Maslen , V. A. Streltsov , N. R. Streltsova , Acta Crystallography B49 **132**, 636 (1993).
[20] S. Miyauchi , H. Imoto , K. Naka , Polymer Journal **48** (1), 1019 (2016).
[21] L. B. Gower , Biomimetic model systems for investigating the amorphous precursor pathway and its role in biomineralization. Chem. Rev. **108** (11), 4551(2008).
[22] Y. Tanaka , K. Naka , Polymer Journal **42** (11), 676 (2010).
[23] S. M. Antao, H. Ishmael, *The Canadian Mineralogist* **48** (5), 1225 (2010).
[24] D. R. Spearing , I. Farnan , J. F. Stebbins , Physics and Chemistry of Minerals **19**, 307 (1992).
[25] B. Mason , L.G. Berry , ''Elements of mineralogy'', A Series of books in Geology QE**363** (M37) (1968).
[26] H. Okuderaa , A. Hozumi , Thin Solid Films **434**, 62 (2003).
[27] A. C. Genevrier , M. Gich , L. Picas , J. Gazquez , G.L. Drisko , C. Boissiere , D. Grosso , J. R. Carvajal , C. Sanchez , Science **340**(827), (2013).
[28] G. L. Drisko , A. C. Genevrier , M. Gich , J. Gàzquez , D. Ferrah , D. Grosso , C. Boissière , J. R. Carvajal , C. Sanchez , Advanced Function Mater **24**, 5494 (2014).
[29] J. Götze , M. Plötze , T. Graupner , D. K. Hallbauer , C. J. Bray, Geochimica , CosmochimicaActa **68**(18), 3741(2004).
[30] B. G. Rusk , M. H. Reed , J. H. Dilles , A. J. R. Kent , American Mineralogist **91**(8-9), 1300 (2006).
[31] A. L. Jourdan , T. W. Vennemann , J. Mullis , K. Ramseyer , C. J. Spiers, European Journal of Mineralogy **21**(1), 219 (2009).
[32] K. Lehmann , A. Berger , T. Götte , K. Ramseyer , M. Wiedenbeck , Mineralogical Magazine **73**(4), 633 (2009).
[33] H.U. Bambauer , Mineralogische und Petrographishe Mitteilungen **41**, 335 (1961).
[34] W. H. Dennen , Geological Society of America Bulletin **78**(1), 125 (1967).
[35] Z. Walenczak , Archiwum Mineralogiezne **28**(0002), 190 (1969).
[36] V. V. Lyakhovich , Izd. Nedra , Moscow, **200** (1972).
[37] S. Beddiaf , S. Chihi , Y. Leghrieb , Journal of African Earth Sciences **106**, 129 (2015).
[38] F. B. Reig , J. V. G. Adelantado , M. C. Moreno , Application to geological samples **58**, 811 (2002).
[39] JCPDS data Philips X'Pert High Score Package, International Center for Diffraction Data, Newtown Square PA (2011).
[40] F. Munawaroh , L. K. Muharrami , T. Kantoro , Z. Arifin , ICBSA, **98** (2019).
[41] B. J. Saikia , G. Parthasarathy , N. C. Sarmah , Bulletin of Materials Science **31**(5), 775 (2008).
[42] B. F. Pederson , D. Semmingsen , ActaCrystallographica Section B **38**, 1074 (1982).
[43] C. Yao , A. Xie , Y. Shen , J. Zhu , T. Li , Journal of the Chilean Chemical Society **58** (4), 2235 (2013).
[44] G. Anbalagan , A. Prabakaran , S. Gunasekaran , Journal of applied spectroscopy **77**(1), 86 (2010).
[45] F. A. Andersen , L. Brecevic , ActaChemicaScandinavica **45**, 1018 (1991).
[46] N. Mahdadi , S. Chihi , H. Bouguettaia , S. Beddiaf , M. L. Mechri , Silicon **9**(2), 211 (2017).
[47] R. L. Frost , J. T. Kloprogge , Z. Ding , The Garfield and Uleynontronites-an infrared spectroscopic comparison, SpectrochimicaActa **Part A** (58), 1881 (2002).
[48] J. Madejova , Vibrational spectroscopy **31**(1), 1 (2003).

[49] B. Hasan , A. Sedat , Ö. E. Serhan , G. Hale , N. C. S. Emine, Materials Letters **58**(723), (2004).
[50] Sh. Fu , Q. Lan , J. Yan , Ore GeologyReviews **126**, 103732 (2020).
[51] M. P. Davidson , G. H. Symmes , B. A. Cohen , R. J. Reeder , D. H. Lindsley, Geochimica , CosmochimicaActa **57** (23-24), 5105 (1993).
[52] N. Meftah , M. S. Mahboub , Silicon **12**, 147 (2020).
[53] S. Chraibi , H. Moussout , F. Boukhlifi , H. Ahlafi , M. Alami , journal of Encapsulation and Adsorption sciences **6**(4), 132 (2016).
[54] Y. Liu , H. Xu , G. Wu ,Chemistry Select **5**(31), 9709 (2020).
[55] F. S. Kodeh , I. M. El-Nahhal , E. A. Elkhair , A. H. Darwish , Chemistry Africa (2019).
[56] J. A. Weil , Physics and Chemistry of Minerals, **10**, 149 (1984).
[57] J. A. Weil , The Physics and Chemistry of SiO2 and the Si-SiO2 Interface **2**, 131 (1993).
[58] S. Beddiaf , S. Chihi , Y. Leghrieb , Journal of African Earth Sciences **106** (129), (2015).
[59] N. Meftah , M. S. Mahboub , Silicon **12**(1), 147 2020
[60] P. S. Nachrichten , V. D. Gesellschaft , D . W. Göttingen , Mathematisch-Physikalische Klasse, **2**, 98 (1918).
[61] A. Sdiri , T. Higashi , T. Hatta , F. Jamoussi , N. Tase , Environmental Earth Science **61**, 1275 (2010).
[62] S. Benchaa , R. Gheriani , A. E. Achouri , H. Bouguettaia , M. L. Mechri , *Arabian Journal of Geosciences* **14** (2265), 1 (2021).
[63] K. Hadjadj, I. Chihi , Silicon **14** (429), (2020).
[64] S. Addala , L. Bouhdjer , A. Chala , A. Bouhdjar , O. Halimi , B. Boudine , M. Sebais , Chinese Physics B **22**(9), 098103 (2013).